RSC Advances

PAPER

View Article Online
View Journal | View Issue

Cite this: *RSC Adv.*, 2024, **14**, 32661

The use of peanut shells as a bio-template to prepare K-doped In_2O_3 porous sheets for chlorine detection†

Lin Zhu *[a] and Heyong Han[b]

Received 18th July 2024
Accepted 27th September 2024

DOI: 10.1039/d4ra05208k

rsc.li/rsc-advances

Chlorine (Cl_2) is highly toxic and pungent, and can cause irreversible harm to humans even at low concentrations. Therefore, it is significant to develop a sensor that is highly sensitive to trace amounts of Cl_2 leakage. In this work, inexpensive peanut shells are used as a biological template to prepare K-doped indium oxide (K-In_2O_3) porous sheets through a simple three-step process. The characterization results reveal the porous sheet microstructure of the prepared K-In_2O_3 derived from the peanut shell bio-template, and the obtained material possesses rich oxygen vacancies and a high specific surface area. Gas-sensing tests demonstrate that the K-In_2O_3 porous sheet sensor exhibits excellent sensitivity to low concentrations of Cl_2.

1 Introduction

Chlorine (Cl_2) is significant to our daily life, and is commonly used as an effective sterilization agent. Additionally, Cl_2 is widely used in industrial and medical applications. In industry, it is employed in the production of chemicals such as oxalic acid, chlor-alkali, and disinfectants. In the medical field, Cl_2 is used to clean and disinfect medical devices. However, Cl_2 also poses various potential hazards because it is a toxic gas with a yellow-green colour and a strong irritating odour. If low concentrations of Cl_2 are inhaled for a sustained period of time, they will cause harm to human skin, mucous membranes, and respiratory and gastrointestinal systems. In severe cases, coma and even death can occur.[1] Therefore, the development of a Cl_2 gas sensor is of great significance. Efficient detection of toxic gases has been a continuous focus of scientific researchers.[2]

A gas-sensing material is the key component used by gas sensors for direct measurement.[3,4] Thus far, various Cl_2-sensing materials based on metal oxides have been reported, such as ZnO,[5] In_2O_3,[6] WO_3,[7] and SnO_2.[8] There are many methods for preparing gas-sensing materials based on metal oxide, including electrospinning,[9] the hydrothermal method,[10] chemical vapor deposition,[11] the sol–gel method,[12] the microemulsion method,[13] the template method,[14] *et al.*[15] Among these, the template method has attracted attention for its diversity, controllability, low cost, and ease of operation.[16] Furthermore, the bio-template method utilizes naturally formed complex structures of biomolecules to achieve precise control and customization of synthetic material structure and properties.[17,18] Thus, the bio-template method can produce new materials with specific functionalities and performances. Additionally, due to the diverse morphology, inexpensive and easy removal, and renewability of biomolecules, the bio-template method is regarded as a promising research focus in nanomaterial synthesis.[19,20]

In this work, peanut shells were used as a bio-template to prepare potassium-doped indium oxide (K-In_2O_3) for Cl_2 detection. Peanut shells are mainly composed of cellulose and lignin, and their fiber contains hydroxyl groups, which are a green, inexpensive, and hydrophilic bio-template.[21] Characterization by scanning electron microscopy (SEM) proved that K-In_2O_3 exhibits a porous sheet-like structure. The Brunauer–Emmett–Teller (BET) results indicated a relatively high surface area for the K-In_2O_3 porous sheets, which was attributable to the use of peanut shell templates. The gas-sensing test results demonstrated that the K-In_2O_3 porous sheets showed satisfactory gas response and excellent selectivity to low concentrations of Cl_2. The superior Cl_2-sensing properties were mainly attributed to the porous sheet-like microstructure and large surface area of the K-In_2O_3 porous sheets that were prepared by the peanut shell bio-template method.

2 Materials and methods

2.1 Synthesis

First, 2.0 g of indium(III) nitrate [$In(NO_3)_3 \cdot 4.5H_2O$] (Innochem Co., Ltd, 99.9%) was added to 80 mL of deionized (DI) water. Next, small pieces of peanut shells (3.0 g) were soaked in the above mixture at room temperature for 0.5 d. Afterward, the

[a]School of Materials Science and Engineering, Taiyuan University of Science and Technology, Taiyuan 030024, China. E-mail: tyustcl@126.com

[b]School of Mechanical Engineering, Taiyuan University of Science and Technology, Taiyuan 030024, China

† Electronic supplementary information (ESI) available. See DOI: https://doi.org/10.1039/d4ra05208k

peanut shells were dried at 80 °C for 14 h. Finally, K-In_2O_3 porous sheets were obtained by calcination of the dried peanut shells at 550 °C for 3 h. In addition, pure In_2O_3 was prepared using the same synthetic process, except that the peanut shells were treated with 100 mL of 1 M hydrochloric acid (HCl) (Sinopharm Chemical Reagent Co., Ltd, 36 wt%) for 2 d. The prepared process is illustrated in Fig. 1.

2.2 Characterization

The phase of the K-In_2O_3 porous sheets was analyzed by X-ray diffraction (XRD, Rigaku Miniflex 600). The microstructure was determined by scanning electron microscopy (SEM, FEI Talos F200X G2). The chemical state was characterized by X-ray photoelectron spectroscopy (XPS, Thermo Scientific ESCALAB 250Xi). The specific Brunauer–Emmett–Teller (BET) surface area was measured using a microporous physisorption instrument (Micromeritics ASAP 2460).

2.3 Gas-sensing testing

First, a paste of sensing material and terpilenol was applied onto the surface of an alumina tube. Second, the sensor was calcinated at 300 °C for 2 h. Third, four platinum wires on the alumina tube and the additional heating wire were attached to the base using a soldering iron. Then, the base was placed on the aging apparatus (Weisheng, TS-60). Last, the gas sensing properties were tested by employing the testing system (Weisheng, WS-30A). The gas response was defined as $|R_{gas}/R_{air}|$ (>1), where R_{gas} and R_{air} denote the resistance in the tested gas and air, respectively.

3 Results and discussion

3.1 Characterization

The crystal structure of K-In_2O_3 fabricated with peanut shells as a bio-template was characterized by XRD, and the result is illustrated in Fig. 2. The peanut shells were not acid treated, and therefore, it was expected that the resultant In_2O_3 would contain elemental K as well. However, because the K content in peanut shells is low, peaks of K were not observed in the XRD pattern. The diffraction peaks of K-In_2O_3 aligned well with those of the standard card (ICDD file no. 00-006-0416),[22,23] indicating a cubic crystal structure.

To observe the microstructure of the K-In_2O_3 fabricated by the peanut shell bio-template method, SEM was performed.

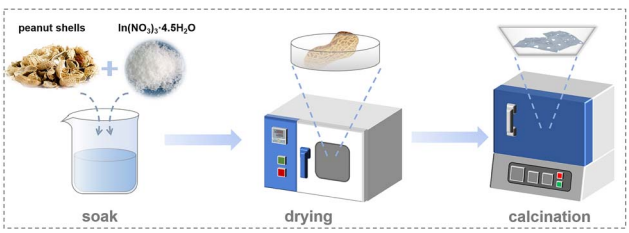

Fig. 1 Schematic diagram of the preparation process for the K-In_2O_3 porous sheets.

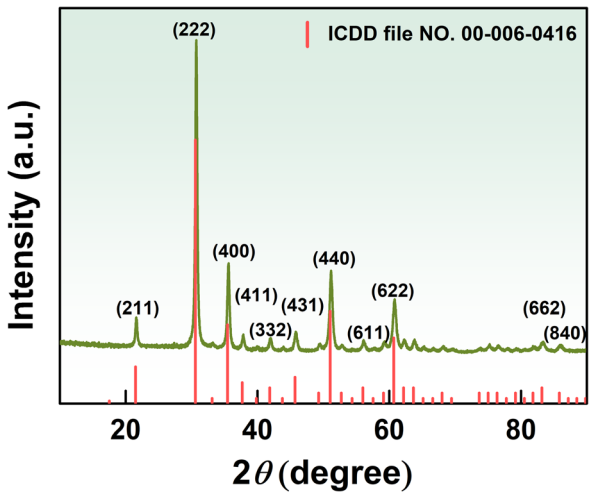

Fig. 2 XRD pattern of the K-In_2O_3 porous sheets.

Fig. 3(a) shows that the morphology of the K-In_2O_3 synthesized using peanut shells as a bio-template exhibits a skeletal structure. The skeletal structure mainly inherits the microstructure of peanut shells. Fig. 3(b) reveals that the skeletal structure is formed by the accumulation of many sheets, while the surface of the sheets is densely packed with particles. The layered surface exhibits numerous irregularly shaped pores, as shown in Fig. 3(c), which may be due to the removal of the bio-template during the calcination process. From Fig. 3(d), it is apparent that the layers are arranged in overlapping sheets with gaps. Thus, the morphology of the K-In_2O_3 porous sheets is largely inherited from that of the peanut shells.

XPS characterization was performed to further determine the elemental composition of the material, and the result is illustrated in Fig. 4. The XPS survey spectrum (Fig. 4(a)) verifies that the K-In_2O_3 porous sheets synthesized using peanut shells as the bio-template mainly consist of In, O, and K elements. The C 1s peak located at 284.6 eV is an external carbon source for calibration. No other elemental peaks were detected in the XPS survey spectrum. This indicates that the K-In_2O_3 porous sheets

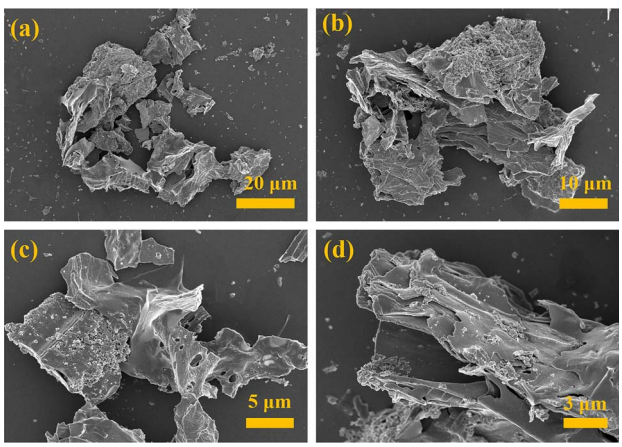

Fig. 3 SEM image of the K-In_2O_3 porous sheets.

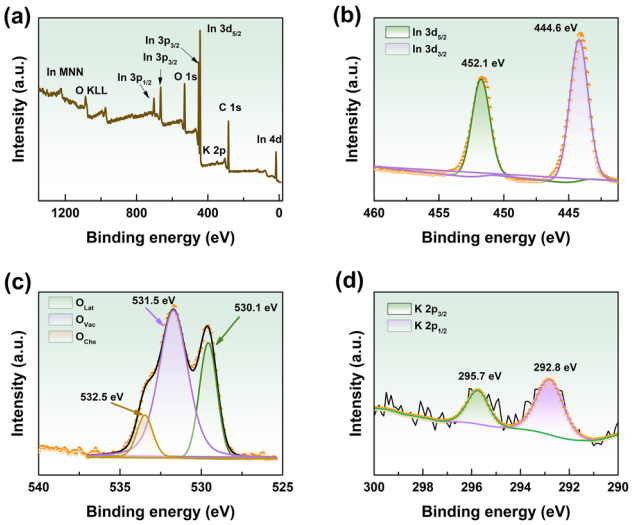

Fig. 4 XPS survey spectra of the K-In_2O_3 porous sheets: (a) fully scanned spectra, (b) In 3d, (c) O 1s, and (d) K 2p.

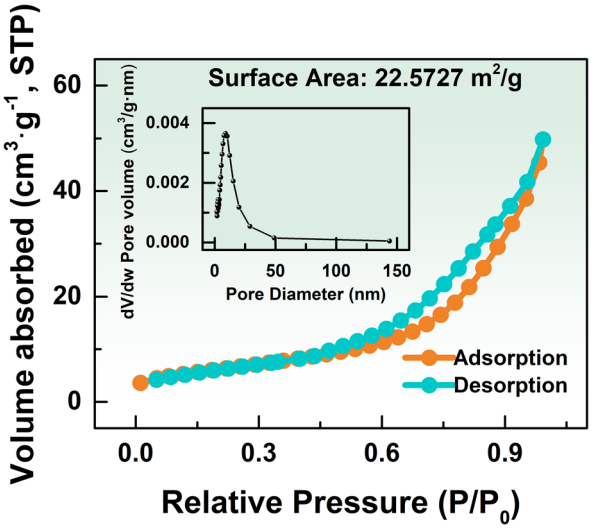

Fig. 5 N_2 isothermal adsorption/desorption isotherms (the inset shows the BJH pore size distribution plot).

were pure, which is in agreement with the XRD analysis. The high-resolution In 3d spectrum is exhibited in Fig. 4(b), and the two peaks at 451.3 eV and 443.8 eV correspond to In $3d_{5/2}$ and In $3d_{3/2}$, respectively. The spin–orbit splitting of 7.5 eV matches the standard values for In_2O_3.[24]

Fig. 4(c) presents the high-resolution O 1s spectrum, with peaks at 530.1 eV, 531.5 eV, and 532.5 eV relating to lattice oxygen, oxygen vacancies, and hydroxyl groups, respectively.[6] Obviously, the concentration of oxygen vacancies is high. The reason for this may be ascribed to the consumption of oxygen and the production of CO_2 during the calcination of the peanut shell template,[25] where a low oxygen atmosphere facilitates the generation of oxygen vacancies.[26] Oxygen vacancies are significant for gas-sensing performance and are components in the gas-sensing mechanism. Additionally, the K 2p peak was found in the fully scanned XPS spectra (Fig. 4(a)). As shown in Fig. 4(d), there are two peaks in the K 2p spectrum at 292.8 and 295.7 eV, which correspond to K $2p_{3/2}$ and K $2p_{1/2}$, respectively.[27] This indicates the K-doping of In_2O_3 (K-In_2O_3) that was prepared by the peanut shell bio-template method. The content of K calculated using the atomic percentage of the XPS results is 9.7%. Fig. S1† shows the XPS spectrum of the pure In_2O_3 that was prepared by the acid-leached peanut shell bio-template method, and indicates that the obtained In_2O_3 does not contain elemental K.

Fig. 5 shows the nitrogen adsorption–desorption curve of the K-In_2O_3 porous sheets synthesized using peanut shells as the bio-template. The isotherm exhibits an H3-type pattern,[28] which lacks a distinct saturation plateau, and indicates that the pore structure is highly irregular. H3-type isotherms are commonly observed in aggregates of layered structures, resulting in slit-shaped mesopores or macroporous materials. These networks consist of large pores that are not filled by pore condensates. As depicted in Fig. 5, the BET surface area of the K-In_2O_3 porous sheets is 22.5727 $m^2\ g^{-1}$. The pore size distribution (the inset of Fig. 5) illustrates that the average pore diameter of the K-In_2O_3 porous sheets is approximately 12.4 nm, which is in the mesopore range.[29]

3.2 Gas-sensing performance

The gas-sensing properties of a gas sensor based on a metal oxide semiconductor mainly depend on the operating temperature. In other words, the working temperature is the most critical factor for gas-sensing properties. Consequently, the optimal operation temperature was determined to assess the gas-sensing performance of the K-In_2O_3 porous sheets prepared using peanut shells as the bio-template. Fig. 6(a) and (b) exhibit the dynamic response curves and sensitivity of the K-In_2O_3 porous sheet sensor to 0.5 ppm Cl_2 at various temperatures, respectively. The result of Fig. 6(b) reveals that with increasing operating temperature, the sensitivity decreases by degrees, and the recovery process becomes increasingly complete.

Considering the sensitivity and the recovery degree, the optimal working temperature for the K-In_2O_3 porous sheet sensor was determined to be 240 °C. Thus, all subsequent gas-sensing tests were conducted at 240 °C. The inset in Fig. 6(b) shows that the response and recovery times for 0.5 ppm Cl_2 at 240 °C are 32 s and 58 s, respectively. According to a previous study,[22] it is generally observed that the lower the gas concentration, the longer the response/recovery times. Therefore, the response/recovery times for the K-In_2O_3 porous sheet sensor at 0.5 ppm Cl_2 are acceptable. The gas-sensing properties of the pure In_2O_3 sensor were also investigated. Fig. S2† shows that the gas response of the pure In_2O_3 sensor to 0.5 ppm Cl_2 was low (<2) at various working temperatures. Thus, the gas-sensing properties of the K-In_2O_3 porous sheet sensor were superior to those of the pure In_2O_3 sensor, and demonstrated that the K content greatly affects the gas-sensing performance.

In practical gas detection, selectivity is the ability of sensors to recognize a specified gas. Therefore, selectivity is another crucial indicator for gas detection, and the gas-sensing

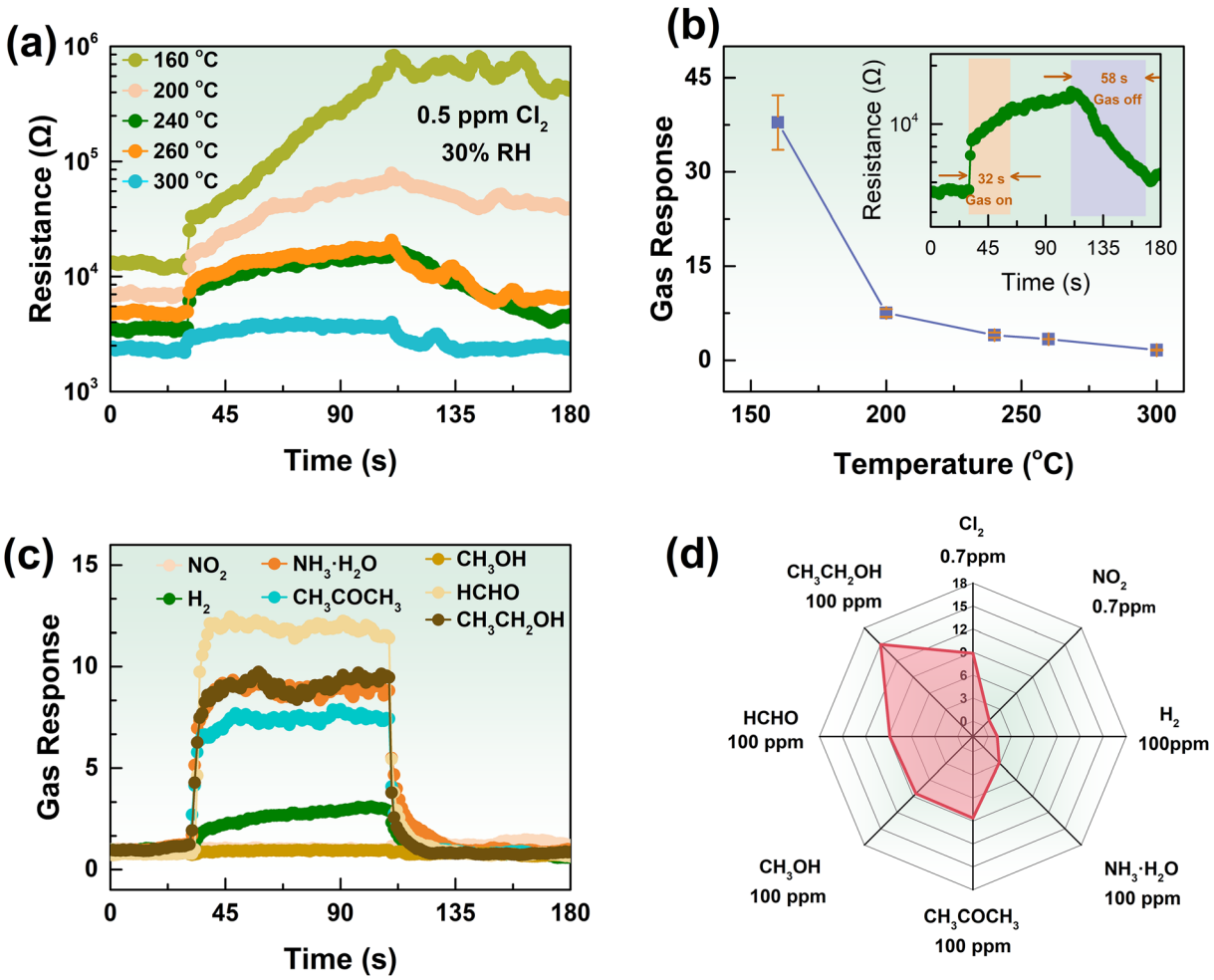

Fig. 6 (a) Dynamic resistance curves and (b) sensitivity to 0.5 ppm Cl_2 at various working temperatures (the inset of (b) is the response/recovery time curve); (c) dynamic response curves and (d) response values to various gases by the K-In_2O_3 porous sheet sensor.

properties of the K-In_2O_3 porous sheet sensor were tested using oxidizing gases (Cl_2, NO_2) and reducing gases (H_2, $NH_3 \cdot H_2O$, CH_3COCH_3, CH_3OH, HCHO, CH_3CH_2OH). Fig. 6(c) displays the transient response curves of the K-In_2O_3 porous sheet sensor to 0.7 ppm oxidizing gases and 100 ppm reducing gases at 240 °C. Fig. 6(d) presents a radar chart of the response values to various gases at different concentrations. The gas response of the K-In_2O_3 porous sheet sensor to Cl_2 was significantly higher as compared to the response to other gases, demonstrating its excellent selectivity.

Furthermore, an excellent gas sensor can detect low concentrations of hazardous gas.[30] Thus, it is ideal for the gas sensor to exhibit a significant response at low concentrations. To investigate the lowest limit of detection (LOD), the gas-sensing properties of the K-In_2O_3 porous sheet sensor were tested under the optimum working temperature of 240 °C with various concentrations of Cl_2. Fig. 7(a) exhibits the dynamic resistance curves of the K-In_2O_3 porous sheet sensor for 0.1–1.0 ppm Cl_2. Fig. 7(b) illustrates the sensitivity of the K-In_2O_3 porous sheet sensor to a series of Cl_2 concentrations. From Fig. 7(a) and (b), as the concentration of Cl_2 increases, the gas response becomes increasingly intense. However, as the concentration of Cl_2 reaches a certain level, the recovery of the sensor becomes less ideal. The inset in Fig. 7(b) demonstrates the satisfactory linear relationship between the logarithm of the sensitivity and the logarithm of the Cl_2 concentration. The LOD for Cl_2 was calculated to be 106.8267 ppb for the K-In_2O_3 porous sheet sensor.

As is well known, Cl_2 is highly soluble in water and also reacts with water,[31] which complicates the detection of chlorine gas. Thus, it was necessary to test the Cl_2 sensing performance under various levels of humidity. Fig. 7(c) and (d) show the transient response curves and sensitivity of the K-In_2O_3 porous sheet sensor, respectively, for 0.7 ppm Cl_2 under 25–75% relative humidity (RH). As illustrated in Fig. 7(c), with increasing humidity, the response value of the K-In_2O_3 porous sheet sensor gradually decreased. Fig. 7(d) reveals that the sensitivity significantly decreased as the RH increased from 25% to 35%. Subsequently, the sensitivity to Cl_2 exhibited a uniform decreasing trend within the higher humidity range of 35% RH to 55% RH. Under high humidity (65% RH to 75% RH), the sensitivity stabilized and greatly decreased.

In practical detection processes, the service life of gas sensors is also a vital element.[32] If the service life is too short, it

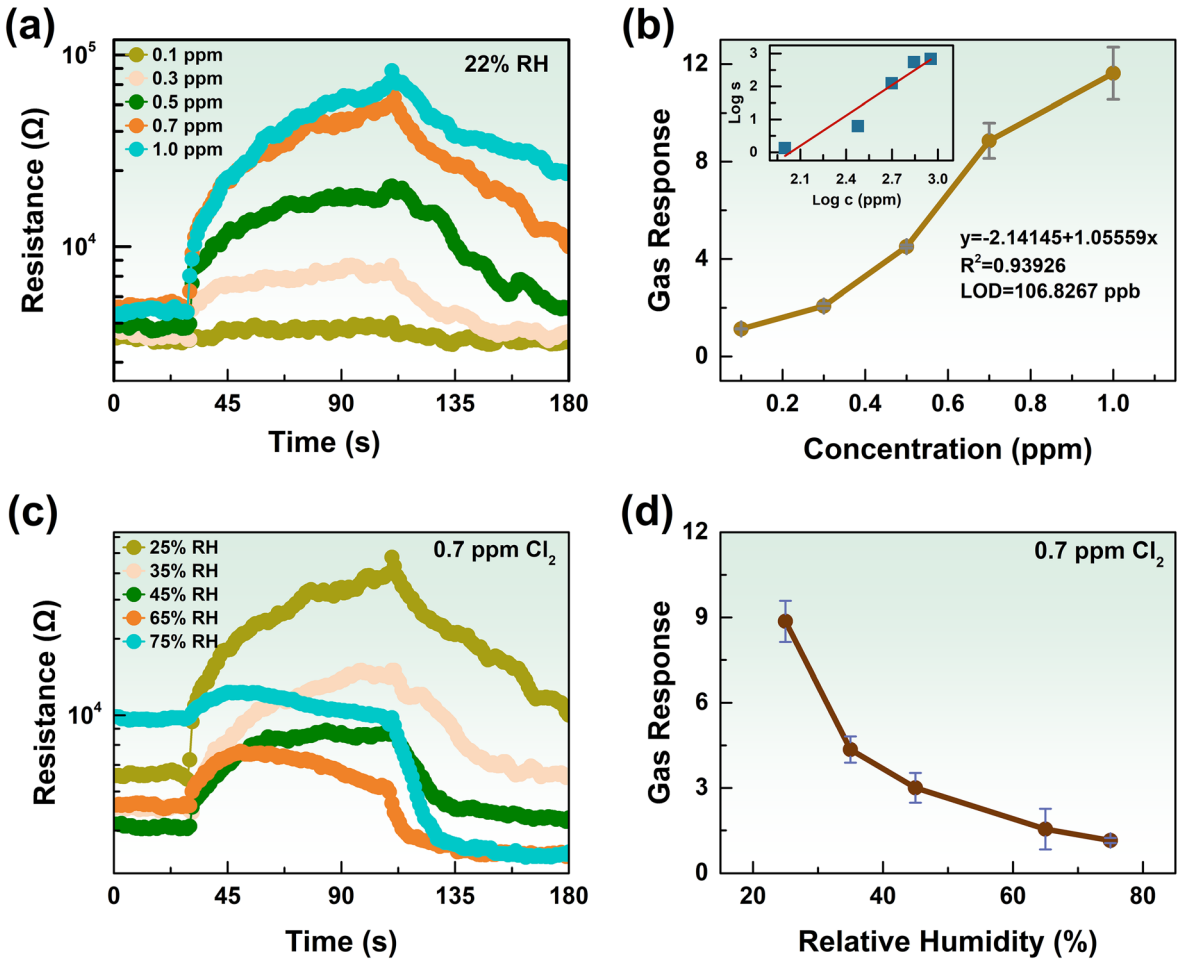

Fig. 7 (a) Dynamic resistance curves and (b) sensitivity to a series of concentrations of Cl_2 at 240 °C (the inset of (b) is the double logarithmic curve); (c) dynamic resistance curves and (d) response value to 0.7 ppm Cl_2 at different levels of humidity.

will be necessary to frequently replace the gas sensor, which is inconvenient. Moreover, if the gas sensor is not replaced in a timely manner, it may result in inaccurate detection and even cause accidents. Therefore, the service life is an indispensable performance indicator in practical detection applications. Systematic gas-sensing tests for the K-In_2O_3 porous sheet sensor were conducted over different days. Fig. 8(a) and (b) display the gas-response transient curves and the response value of the K-In_2O_3 porous sheet sensor for 0.7 ppm Cl_2 at different times, respectively. As observed in Fig. 8(b), the sensitivity of the K-

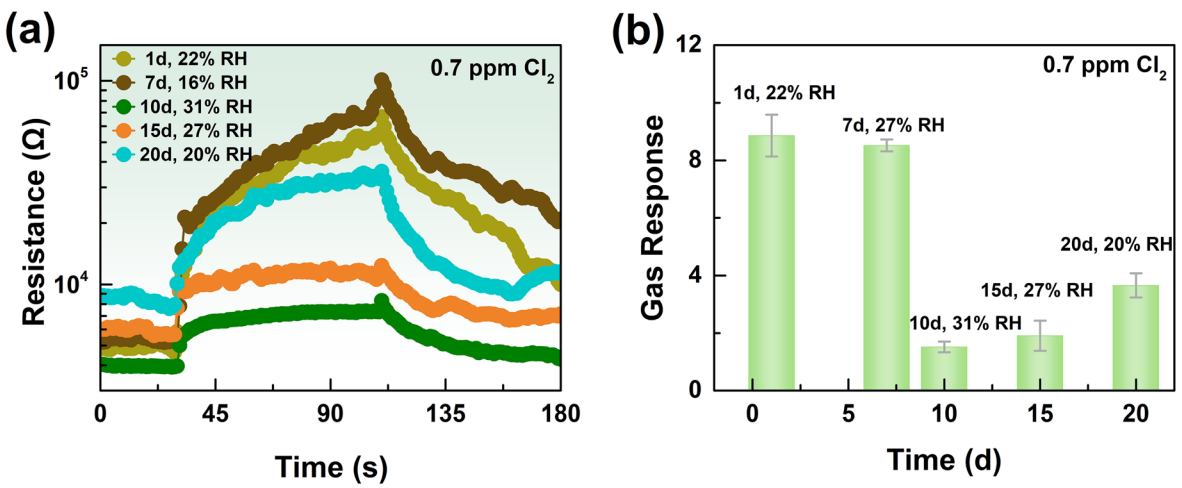

Fig. 8 (a) Dynamic resistance curves and (b) sensitivity to 0.7 ppm Cl_2 at different times.

Table 1 Comparison of the Cl_2-sensing properties of In_2O_3 sensors

Sensor	Method	BET surface area ($m^2\ g^{-1}$)	Complexity/cost	T (°C)	Cl_2 (ppm)	Gas response
In_2O_3 microstructures[33]	Hydrothermal method	0.0081	Simple/normal	300	100	1385
Fe_2O_3–In_2O_3 porous sheets[34]	Hydrothermal method	0.5328	Simple/normal	300	100	1739
In_2O_3 mesoporous[35]	Hydrothermal method	0.0034	Simple/normal	260	100	1540
In_2O_3 hollow microtubules[36]	Degreasing cotton bio-template	11.6500	Simple/low	200	10	1051
In_2O_3 microspheres[25]	Yeast bio-template	9.9000	Simple/low	240	10	96
Fe_2O_3–In_2O_3 thin film[37]	Electron beam evaporation	—	Complex/high	400	5	69
In_2O_3 porous sheets (this work)	Peanut shell bio-template	22.5727	Simple/low	240	0.5	3.97

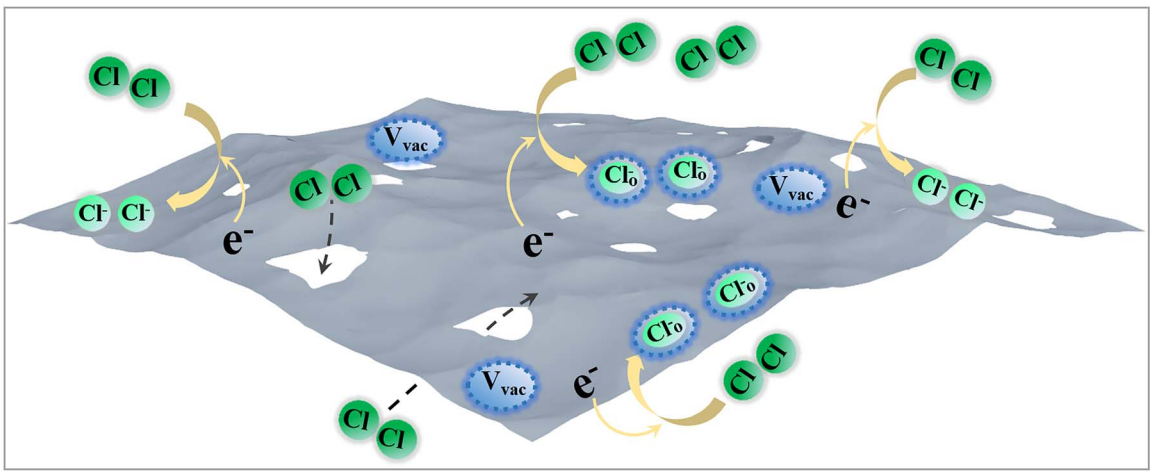

Fig. 9 A diagram of the gas-sensing mechanism.

In_2O_3 porous sheet sensor to Cl_2 is significantly influenced by the working time and the environmental humidity, which is a challenge for Cl_2 sensors in practical applications. Stability tests were conducted over 20 days under varying times and humidities, and although the response value of the K-In_2O_3 porous sheet sensor to Cl_2 decreased with working time, notable sensitivity was maintained. Thus, the general stability of the K-In_2O_3 porous sheet sensor synthesized using peanut shells as a bio-template has been demonstrated.

Lastly, a comparison of Cl_2-sensing properties of In_2O_3 sensors is given in Table 1. Compared to other preparation methods, the peanut shell bio-template method is simple, easy to perform, and cost-efficient. Additionally, the BET surface area of the K-In_2O_3 porous sheets prepared by the peanut shell bio-template method was larger than that of In_2O_3 synthesized by hydrothermal methods, electron beam evaporation, and other bio-template methods. Although the operating temperature was moderate, the sensor based on K-In_2O_3 porous sheets prepared using a peanut shell bio-template is excellent for detection of low concentrations of Cl_2.

3.3 Gas-sensing mechanism

Based on the results of gas-sensing tests, the resistance of the K-In_2O_3 porous sheets (an n-type semiconductor) increased upon exposure to Cl_2 (Fig. 6(a)). The gas-sensing mechanism is deduced as follows:[38,39]

$$Cl_2 + 2e^- \rightarrow 2Cl^- \quad (1)$$

$$Cl_2 + 2\ O_{vac} + 2e^- \rightarrow 2Cl\text{–}O \quad (2)$$

Reaction (1) describes the direct adsorption of Cl_2 molecules to capture electrons. Reaction (2) describes the adsorption of Cl_2 onto oxygen vacancies. In both reactions, electrons are depleted, leading to increased resistance. The gas-sensing mechanism of the K-In_2O_3 porous sheets is schematically displayed in Fig. 9.

The high sensitivity of the K-In_2O_3 porous sheet sensor in the detection of low concentrations of Cl_2 may be ascribed to the following. First, the K-In_2O_3 porous sheets synthesized using the peanut shell bio-template method retained the morphological features of peanut shells. This resulted in a large BET surface area that was favorable for facilitating reaction (1). Second, the formation of CO_2 and H_2O vapour during the calcination of the peanut shells created a temporary low-oxygen environment that promoted the generation of oxygen vacancies in In_2O_3. Consequently, the high concentration of oxygen vacancies in the K-In_2O_3 porous sheets enhanced reaction (2).

4 Conclusions

K-In_2O_3 porous sheets were prepared through a three-step process using the peanut shells as the bio-template. The morphology of the porous sheets was mainly inherited from the

peanut shells. The high concentration of oxygen vacancies and the large BET surface area of the K-In_2O_3 porous sheets were due to the use of the peanut shell bio-template. The K-In_2O_3 porous sheet sensor exhibited an excellent gas response to low concentrations of Cl_2. Based on the analysis of the gas-sensing mechanism, the high specific surface area and abundant oxygen vacancies of the K-In_2O_3 porous sheets are conducive to Cl_2 detection.

Data availability

The data supporting this article have been included within the manuscript and its ESI.†

Author contributions

Lin Zhu: conceptualization, resources, data, curation, formal analysis, supervision, funding acquisition, validation, investigation, visualization, writing – original draft, writing – review and editing. Heyong Han: writing – review & editing.

Conflicts of interest

There are no conflicts to declare.

Acknowledgements

This work was supported by Key Projects of Shanxi Province Key Research and Development Plan (Grant No. 201703D111003) and the Shanxi Province Scientific and Technological Achievements Transformation Guidance Project (Grant No. 202204021301054).

Notes and references

1 C. W. White and J. G. Martin, *Proc. Am. Thorac. Soc.*, 2010, **7**, 257–263.
2 A. K. Saroha, *J. Chem. Health Saf.*, 2006, **13**, 5–11.
3 J. Ma, H. Zhai, Z. Zhang, M. Di, Z. Sun, K. Zhang, J. Hu and H. Fan, *ACS Appl. Nano Mater.*, 2023, **6**, 19797–19806.
4 A. Dey, *Mater. Sci. Eng. B*, 2018, **229**, 206–217.
5 X. Meng, R. Gao, M. Zheng, X. Zhou, X. Zhang, X. Cheng, Y. Xu, S. Gao and L. Huo, *Chem. Eng. J.*, 2024, **493**, 152631.
6 J. Ma, H. Fan, W. Zhang, J. Sui, C. Wang, M. Zhang, N. Zhao, A. Kumar Yadav, W. Wang, W. Dong and S. Wang, *Sens. Actuators, B*, 2020, **305**, 127456.
7 F. Bender, C. Kim, T. Mlsna and J. F. Vetelino, *Sens. Actuators, B*, 2001, **77**, 281–286.
8 J. Ma, H. Fan, X. Ren, C. Wang, H. Tian, G. Dong and W. Wang, *ACS Sustainable Chem. Eng.*, 2019, **7**, 147–155.
9 S. Ma and J. Xu, *J. Mater. Chem. A*, 2023, **11**, 23742–23771.
10 T. T. Nguyet, D. T. Thanh Le, N. Van Duy, C. T. Xuan, S. Ingebrandt, X. T. Vu and N. D. Hoa, *RSC Adv.*, 2023, **13**, 13017–13029.
11 V. S. Bhati, M. Kumar and R. Banerjee, *J. Mater. Chem. C*, 2021, **9**, 8776–8808.
12 S. M. Majhi, S. T. Navale, A. Mirzaei, H. W. Kim and S. S. Kim, *Inorg. Chem. Front.*, 2023, **10**, 3428–3467.
13 N. Baig, I. Kammakakam and W. Falath, *Adv. Mater.*, 2021, **2**, 1821–1871.
14 T. Xu, J. Zhao, F. Zhao, W. Cong and G. Wang, *Sens. Actuators, B*, 2023, **394**, 134338.
15 Z. Wang, L. Zhu, J. Wang, R. Zhuang, P. Mu, J. Wang and W. Yan, *RSC Adv.*, 2022, **12**, 24614–24632.
16 B. Y. Song, C. Li, X. F. Zhang, R. Gao, X. L. Cheng, Z. P. Deng, Y. M. Xu, L. H. Huo and S. Gao, *J. Mater. Chem. A*, 2022, **10**, 14411–14422.
17 T. Xu, H. Wang, J. Zhao, F. Zhao, W. Cong, G. Wang and J. Li, *Dalton Trans.*, 2023, **52**, 10835–10843.
18 P. Song, H. Zhang, D. Han, J. Li, Z. Yang and Q. Wang, *Sens. Actuators, B*, 2014, **196**, 140–146.
19 M. B. Guerrero, J. M. Valverde, A. Perejon, P. E. S. Jimenez and L. A. P. Maqueda, *Appl. Energy*, 2018, **210**, 108–116.
20 T. Chen, M. Li, S. Song, P. Kim and J. Bae, *Nano Energy*, 2020, **71**, 104549.
21 J. Zhou, Y. Guo, C. Liang, J. Yang, J. Wang and Y. Nuli, *Electrochim. Acta*, 2018, **273**, 127–135.
22 K. K. Pawar, L. S. Chaudhary, S. S. Mali, T. S. Bhat, A. D. Sheikh, C. K. Hong and P. S. Patil, *J. Colloid Interface Sci.*, 2020, **561**, 287–297.
23 H. Wang, G. Fan, Z. Yang, N. Han, Y. Chen and J. Yang, *ACS Appl. Nano Mater.*, 2022, **5**, 7983–7992.
24 J. Mu, B. Chen, M. Zhang, Z. Guo, P. Zhang, Z. Zhang, Y. Sun, C. Shao and Y. Liu, *ACS Appl. Mater. Interfaces*, 2012, **4**, 424–430.
25 J. Ma, H. Fan, N. Zhao, W. Zhang, X. Ren, C. Wang, Y. Wen and W. Wang, *Ceram. Int.*, 2019, **45**, 9225–9230.
26 L. Liu, F. Gao, H. Zhao and Y. Li, *Appl. Catal., B*, 2013, **134–135**, 349–358.
27 X. Lu, D. Zhang, J. Zhong, L. Wang, L. Jiang, Q. Liu, G. Shao, D. Fu, J. Teng and W. Yang, *Chem. Eng. J.*, 2022, **432**, 134416.
28 K. S. W. Sing, *Pure Appl. Chem.*, 1985, **57**, 603–619.
29 J. C. Groen, L. A. A. Peffer and J. P. Ramírez, *Microporous Mesoporous Mater.*, 2003, **60**, 1–17.
30 R. Kumar, O. A. Dossary, G. Kumar and A. Umar, *Nano-Micro Lett.*, 2015, **7**, 97–120.
31 G. L. Squadrito, E. M. Postlethwait and S. Matalon, *Am. J. Physiol. Lung Cell Mol. Physiol.*, 2010, **299**, 289–L300.
32 A. C. Romain and J. Nicolas, *Sens. Actuators, B*, 2010, **146**, 502–506.
33 P. Li and H. Fan, *Mater. Sci. Semicond. Process.*, 2015, **29**, 83–89.
34 P. Li, Y. Cai and H. Fan, *RSC Adv.*, 2013, **3**, 22239–22245.
35 P. Li, H. Fan and Y. Cai, *Colloids Surf., A*, 2014, **453**, 109–116.
36 J. Ma, H. Fan, H. Tian, X. Ren, C. Wang, S. Gao and W. Wang, *Sens. Actuators, B*, 2018, **262**, 17–25.
37 J. Tamaki, C. Naruo, Y. Yamamoto and M. Matsuoka, *Sens. Actuators, B*, 2002, **83**, 190–194.
38 D. H. Dawson and D. E. Williams, *J. Mater. Chem.*, 1996, **6**, 409–414.
39 T. Van Dang, N. Duc Hoa, N. Van Duy and N. Van Hieu, *ACS Appl. Mater. Interfaces*, 2016, **8**, 4828–4837.